Characterization of Multi-axial Hyperelastic Behavior of Mooney-Rivlin Materials: Results of Finite Element Simulations

Hocine Bechir⋆, Kamel Yaya, and Amar Djema,

Laboratoire de Mécanique, Matériaux et Énergétique (L2ME), Faculté de Technologie, Université de Bejaia, 06000 Bejaia, Algeria

Abstract: The calibration of the parameters of hyperelastic consitutive equations of elastomeric materials requires multi-axial mechanical test data. For this reason, planar biaxial tests have been used extensively in the literature. The drawback of the biaxial tensile test is that difficult to manage and gives raise to heterogeneous stress and strain fields. Noting that, a homogeneous stress-strain field allows for more precise determination of the mechanical properties of a sample. To this end, we present an alternative to biaxial testing, i.e. a novel test protocol that is consisting to deform a sample by coupling both the deformations of pure shear and of simple shear (or rectilinear shear). The sample is oriented in the plane of a special device, which is attached to a universal tensile testing machine. As a result, the stress-strain relations depend on the direction of stretching, i.e. $\Theta \in]0, \pi/2[$ (angle of orientation of the sample in the device) and displacement U (or γ). We compute analytically the Cauchy stresses on the basis of assumption of homogeneous strain field in core region of the sample. We show that, these stresses are almost equal to that arising from the FE simulations. The homogeineity of fields in the core region allows us to relate the Cauchy stresses to the applied forces (under condition that the boundary value problems are well controlled allowing to obtain uniform stresses). So, the experimental data arising from this test could be suitable for identification or/and validation of hyperelastic models.

Keywords: Hyperelasticity, Multi-axial behavior, Test-design, Finite element simulations

1 Introduction

The modeling of hyperelastic behavior of isotropic elastomers is well established in framework of continuum mechanics Ogden (1997); Holzapfel (2000). In many engineering applications, one needs to implement these models in commercial finite element codes. Consequently, the identification is a crucial step, which consists in estimating the constitutive parameters at best from a measured displacement field and applied forces. Due to the complex behavior of elastomeric materials, the model parameter calibration requires complex experimental protocols, from experimental setup and sample (e.g., complex multiaxial loadings, optimized geometry). In the field of solid mechanics, numerous relevant identification and validation strategies have been development in the context of full-field measurements techniques Hild and Roux (2006); Grédiac et al. (2006); Hartmann and Rodriguez (2018) and references cited therein. Standard tests related with this purpose require sample geometries that can lead to homogeneous deformations (uni-axial tensile, pure shear and equi-bi-axial tensile) Sasso et al. (2008); Galliot and Lushinger (2011). In practice, the constitutive parameters that are identified with those three types test performed separately are generally different Guo and Sluys (2006). To bypass the problem, the material parameters could be identified from experimental data of the biaxial tensile test in order to ensure predictive ability of a hyperelastic model Seibert et al. (2014). We emphasize that, the heterogeneous deformation states of equibiaxial tensile test and an inverse method (so-called, the virtual fields method) have been used Promma et al. (2009) in order to compute the Mooney-Rivlin model constants Mooney (1940). We notice that, the computation of deformation and stress states in core region of a cruciform specimen is a subject of debate Hartmann et al. (2018) (and the literature cited therein). The strains distribution seems to be uniform; nevertheless, the corresponding stress distribution does not. We conclude that, biaxial tensile test seems to give rise to heterogeneous stress and strain fields even near core region of a cruciform sample.

In this work, a concept testing was proposed in order to characterize the multi-axial behavior of elastomeric materials. The testing consists of the coupled stretching and shearing instead of performing them separately. The Cauchy stresses have been investigated on the basis of homogeneous strains in central region of the sample made of a Mooney-Rivlin material. The stress-strain relationship depends both on the stretching-direction and amplitude of displacement prescribed on the specimen edge. On the basis of homogeneous strain fields in core region, we could compute analytically both the Cauchy stress and strain fields. We show that, the Cauchy stresses are almost equal to that arising from the FE simulations. As result, the Cauchy stress field could be related to the applied forces (under condition that the boundary value problems are well controlled allowing to obtain uniform stresses). So, the experimental data arising from this test could be suitable for the identification or/and validation of hyperelastic models.

The plan of the paper is as follows: In Section 2, we recall the basic equations of isotropic hyperelasticity. In Section 3, we have investigated analytically the proposed theoretical approach. In Section 4, we have validated the analytical results by using the Finite Element simulations in order to compute the Cauchy stresses distribution in core region of the sample. In section 5, we

draw some concluding and remarks.

2   Basic equations of isotropic hyperelastcity

In continuum mechanics, the mechanical properties of elastomeric materials are described in terms of strain-energy density function Ψ Ogden (1997); Holzapfel (2000). For isotropic elastic material, Ψ depends on the strain principal invariants

$$I_1 = tr(\mathbf{B}),\ I_2 = \frac{1}{2}\left[(tr(\mathbf{B}))^2 - tr(\mathbf{B}^2)\right],\ I_3 = det(\mathbf{B}), \tag{1}$$

where $\mathbf{B} = \mathbf{FF}^t$ is the left Cauchy-Green tensor and $\mathbf{F}$ is the gradient of the deformation.
The deformation gradient is defined by $\mathbf{F} = \partial\mathbf{x}/\partial\mathbf{X}$, $\mathbf{X}$ and $\mathbf{x}$ are the vector location of a material particle in the undeformed and deformed configurations, respectively.
Rubber-like materials are often assumed to be incompressible provided that the hydrostatic stress does not become too large and so the admissible deformations must be isochoric, (i.e., $det\mathbf{F} = 1$), so that, $I_3 = 1$. The Cauchy stress of an incompressible isotropic elastic material can be determined as follows:

$$\boldsymbol{\sigma} = -p\mathbf{I} + 2\Psi_{,1}\mathbf{B} - 2\Psi_{,2}\mathbf{B}^{-1}, \tag{2}$$

where p is the Lagrange multiplier, $\mathbf{I}$ is the identity tensor and $\Psi_{,i} = (\partial\Psi/\partial I_i)_{i=1,2}$ are the partial derivatives of the strain-energy density function.
We consider the phenomenological Mooney-Rivlin model Mooney (1940) which is suitable to predict the behavior of elastomeric materials in the range of moderate strains. The strain-energy density function is as follows:

$$\Psi = \frac{\mu_0}{2}\left[\alpha\left(I_1 - 3\right) + (1 - \alpha)\left(I_2 - 3\right)\right], \tag{3}$$

where μ_0 is the shear modulus for infinitesimal deformations and $\alpha \in]0, 1]$ is a dimensionless constant.

3   The testing design

Denote the unit vectors associated with a fixed Cartesian coordinates system in the reference configuration by $(\mathbf{E}_1, \mathbf{E}_2, \mathbf{E}_3)$ and in the current configuration by $(\mathbf{e}_1, \mathbf{e}_2, \mathbf{e}_3)$. Consider a rectangular plate made of elastomeric material bonded to two rigid plates, with edges aligned with $\mathbf{E}_1$, $\mathbf{E}_2$ and $\mathbf{E}_3$. $L = mH$ denotes the length of the plate, H its height and $m \geq 2$ is the shape factor; e is the thickness of the plate with $H >> e$. Let us to define the new test as shown in Figs. 1 consisting to apply a loading in a direction $\Theta \in]0, \pi/2[$ on the upper face of the plate in $Y = H$; the bottom face of the plate is blocked in $Y = 0$ (no displacement is possible). For $\Theta = \pi/2$, the deformation reduces to that of the pure shear test; if $\Theta = 0$ then the deformation is that of the simple shear (or rectilinear shear). Consequently, the deformation can be decomposed as a superposition of simultaneous deformations in the direction Y (stretching) and in the direction X (shearing). The resulting deformation depends on the angle Θ of stretching. In core region, we may assume that the deformations are quasi-homogeneous (affine), since the length of plate is more important than height ($L \geq 2H$). In other words, the "boundary-effects" can be neglected at far from the edges of the specimen. Accordingly, we may decompose the coupled deformations into two successive deformations: (i) the first one is the quasi-homogeneous (affine) deformation corresponding to the pure shear with the principal stretch ratio, λ, and (ii) one which uses the homogeneous configuration as the reference state, that is, the rectilinear shear. This multiplicative decomposition of the deformation gradient, so-called Successive Decomposition Procedure (SDP) has been applied Mihai and Goriely (2015) in the context of cellular structures. With these assumptions, let us postulate that a homogeneous isotropic and incompressible material is subjected to the following transformation:

$$x = X + \kappa\lambda Y,\ y = \lambda Y,\ z = \frac{Z}{\lambda}, \tag{4}$$

where λ and κ are the stretch ratio along the X_2-axis and local amount of shear, respectively.
Eq.(4) can be viewed as a special case of the transformation that was investigated in Wineman and Ghandi (1984). The deformation gradient tensor $\mathbf{F}$ is inferred from Eq. (4) as follows:

$$\mathbf{F} = \begin{pmatrix} 1 & \kappa\lambda & 0 \\ 0 & \lambda & 0 \\ 0 & 0 & \lambda^{-1} \end{pmatrix} = \begin{pmatrix} 1 & \kappa & 0 \\ 0 & 1 & 0 \\ 0 & 0 & 1 \end{pmatrix} \begin{pmatrix} 1 & 0 & 0 \\ 0 & \lambda & 0 \\ 0 & 0 & \lambda^{-1} \end{pmatrix} = \mathbf{F}^{(1)}\mathbf{F}^{(2)}, \tag{5}$$

where $\mathbf{F}^{(1)}$ and $\mathbf{F}^{(2)}$ are the gradients tensors of deformation corresponding to simple shear and pure shear, respectively. The decomposition of Eq. (5) is similar to the method adopted in finite elastoplasticity (Lee (1969)), in which the local deformation gradient is decomposed into elastic and plastic parts. Also, this multiplicative decomposition was applied with success in viscoelasticity (Reese and Govindjee (1998)), thermoelasticity and biomechanics (Lubarda (2004)). Consequently, this general

H. Bechir, K. Yaya, A. Djema

Tech. Mech., Vol. 40, Is. 1, (2020), 15–21

(a)

(b)
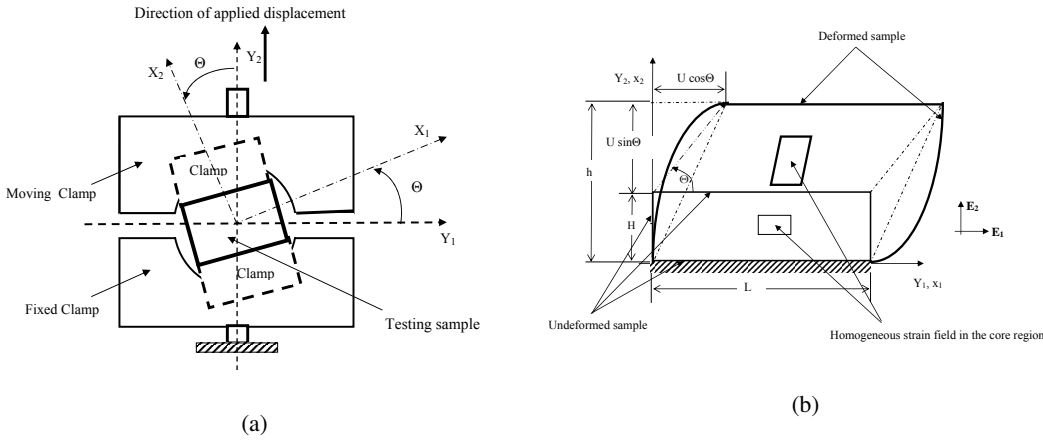
Fig. 1: Schematic representation of the proposed test: (a) the sample is gripped with two clamps, the moving clamp is displacement vertically to induce simultaneously a shearing and stretching of the sample, where $\Theta \in]0, \pi/2[$ is the angle between the principal axes of the sample and the column of the tensile machine. (b) The sample is a thin rectangular sheet of length $L = 0.04m$ width $H = 0.02m$ and of thickness $e = 0.004m$. We represent schematically the deformation that is assumed homogeneous in core region of the sample.

decomposition is carried out to assign various physical causes to kinematical quantities. Noting that the study of state of simple shear, i.e. $\lambda = 1$, had been subject of growing interest (Ogden (1997); Bertram (2008)). Recently, some authors have concluded that "simple shear is not so simple" (Destrade et al. (2012); Horgan and J.G. (2014); and Thiel et al. (2019)). In fact, finite simple shear cannot be maintained by shear stress alone. Normal stresses are needed to maintain the normal strains at zero; this will result in an inhomogeneous field.

Accordingly, we may assume that the stretch ratio is given by

$$\lambda \approx \frac{h}{H} = \frac{H + U \sin \Theta}{H} = 1 + \gamma \sin \Theta, \tag{6}$$

$$\kappa\lambda = \gamma \cos \Theta. \tag{7}$$

The right Cauchy-Green strain tensor and its inverse are as follows:

$$\mathbf{B} = \begin{pmatrix} 1 + \kappa^2\lambda^2 & \kappa\lambda^2 & 0 \\ \kappa\lambda^2 & \lambda^2 & 0 \\ 0 & 0 & \lambda^{-2} \end{pmatrix}, \quad \mathbf{B}^{-1} = \begin{pmatrix} 1 & -\kappa & 0 \\ -\kappa & (1 + \kappa^2\lambda^2)\lambda^{-2} & 0 \\ 0 & 0 & \lambda^2 \end{pmatrix}. \tag{8}$$

Substituting Eq. (3) into Eq. (2) and substituting Eq. (8) into the resulting of Eq. (2), the Cauchy stresses of Mooney-Rivlin model can be expressed as

$$\sigma_{11} = \mu_0 \left[\alpha(1 + \kappa^2\lambda^2 - \lambda^{-2}) + (1 - \alpha)(\lambda^2 - 1) \right], \tag{9}$$

$$\sigma_{12} = \mu_0\kappa((1 - \alpha)\kappa + \alpha\lambda^2), \tag{10}$$

$$\sigma_{22} = \mu_0 \left[\alpha(\lambda^2 - \lambda^{-2}) + (1 - \alpha)(\lambda^2 - (1 + \kappa^2\lambda^2)\lambda^{-2}) \right]. \tag{11}$$

We would to relate the measured force at the edges of the specimen to Cauchy stresses of the core region. The boundary conditions of the testing can be expressed in terms of the components of first Piola-Kirchhoff stress tensor i.e. $\mathbf{P}$, as follows:

$$\mathbf{P} = \begin{pmatrix} 0 & P_{12} & 0 \\ 0 & P_{22} & 0 \\ 0 & 0 & 0 \end{pmatrix}, \tag{12}$$

where $P_{22} = \dfrac{\text{Force}(\gamma; \Theta)}{eL} \sin \Theta$ and $P_{12} = \dfrac{\text{Force}(\gamma; \Theta)}{eL} \cos \Theta$.

Lets us compute the Cauchy stress tensor, i.e., $\boldsymbol{\sigma} = P\mathbf{F}^t$ by using Eqs. (5) and (12)

$$\boldsymbol{\sigma} = \begin{pmatrix} \sigma_{11} & \sigma_{12} \\ \sigma_{12} & \sigma_{22} \end{pmatrix} = \begin{pmatrix} 0 & P_{12} \\ 0 & P_{22} \end{pmatrix} \begin{pmatrix} 1 & 0 \\ \kappa\lambda & \lambda \end{pmatrix} = \begin{pmatrix} \kappa\lambda P_{12} & \lambda P_{12} \\ \kappa\lambda P_{22} & \lambda P_{22} \end{pmatrix}. \tag{13}$$

(a)   (b)   (c)
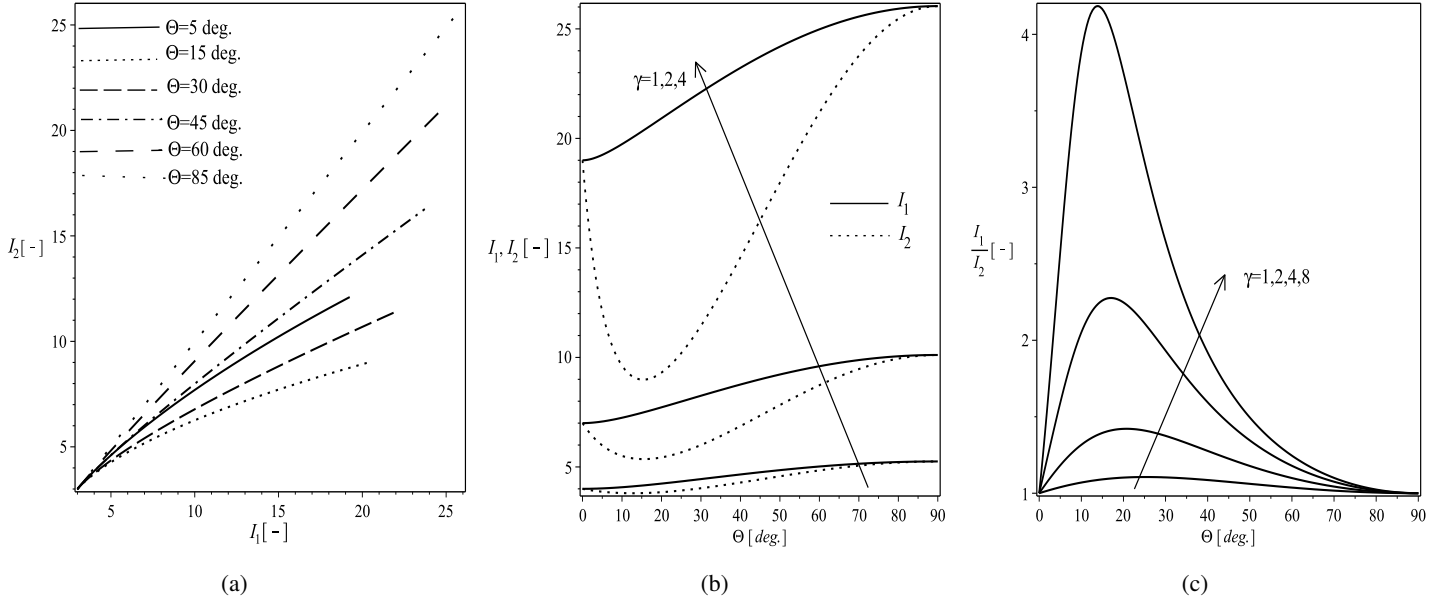
Fig. 2: Plots of the invariants I_2 versus I_1 (a) graphical representation of the plan of invariants, i.e. $I_2(I_1)$, (b) graphical representation of the invariants I_1 and I_2 versus Θ, (c) graphical representation of the ratio I_1/I_2 versus Θ.

So, the Cauchy stresses are as follows:

$$\sigma_{11} = \kappa\lambda\, P_{12}, \sigma_{12} = \lambda\, P_{12} = \kappa\lambda\, P_{22}, \text{ and } \sigma_{22} = \lambda\, P_{22}. \tag{14}$$

Notice that, the parameter γ needs to be chosen sufficiently great in order to satisfy

$$\frac{P_{12}}{P_{22}} = \tan^{-1}\Theta = \lim_{\gamma\to+\infty}\frac{\gamma\cos\Theta}{1+\gamma\sin\Theta}. \tag{15}$$

We can check the validity of the present approach by comparison the predictions of Eqs. (9), (10) and (11) with the results of FE-simulations(See next Section).

We compute the principal invariants of the left Cauchy-Green strain tensor by using Eqs. (6), (7) and (8), and obtain the following expressions:

$$
\begin{aligned}
I_1(\mathbf{B}) &= 1 + \lambda^2 - \lambda^{-2} + \kappa^2\lambda^2 \\
&= \frac{3 + \gamma^2 + 6\gamma(1+\gamma\sin\Theta)\sin\Theta + 2\gamma^3(\cos^2\Theta + 2\sin\Theta)\sin^2\Theta + \gamma^4\sin^2\Theta}{(1+\gamma\sin\Theta)^2},
\end{aligned}
\tag{16}
$$

$$
\begin{aligned}
I_2(\mathbf{B}) &= 1 + \lambda^2 - \lambda^{-2} + \kappa^2 \\
&= \frac{3 + \gamma^2 + 6\gamma(1+\gamma\sin\Theta)\sin\Theta + 4\gamma^3\sin^3\Theta + \gamma^4\sin^4\Theta}{(1+\gamma\sin\Theta)^2}.
\end{aligned}
\tag{17}
$$

When $\Theta = 0$ or $\Theta = \pi/2$, the first and the second invariants are equal. If $\Theta = \pi/2$ then the test reduces to the pure shearing(stretching), and for $\Theta = 0$, it is corresponding to the simple shear testing. We plot in Fig.2(a) the graphical representation of the plan of invariants, i.e. $I_2(I_1)$ for values of $\gamma = 0..4$. The multi-axial state of deformation could be reached by varying the angle Θ, so the corresponding domain represents the admissible deformation state of incompressible elastomeric materials. The graphs of I_1 and I_2 versus θ are shown in Fig. 2(b) for different values of γ. The second invariant, i.e. I_2 strongly changes. According to Horgan and Smayda (2012) it should be included in the strain energies for isotropic materials; while I_1 is an increasing function. The ratios I_1/I_2 are displayed in Fig. 2(c), the curves are nonlinear and their maximums seem to be slightly depending on Θ and γ, and $I_1 > I_2$. We notice that, this "new" testing does not cover the deformation states of the biaxial test, i.e. $I_2 > I_1$. We emphasize that, Baaser et al. (2013) have analyzed the tension modes, i.e. $I_1 > I_2$ in terms of the variables (λ, m) ; the mode of deformation in his representation is dictated by the numerical value of the parameter m.

4 Finite Elements Analysis and Simulations

We study numerically by FE the proposed test in order to highlight the discrepancies between the results of FE-simulations and predictions of Eqs. (9), (10) and (11). A finite element calculation is performed by assuming both plane stress state and a nearly-incompressibility approach. Thus, a mixed formulation pressure-displacement was used in order to avoid element locking.

For that purpose, the strain-energy density function is decomposed into an isochoric and volumetric parts. To this end, we declare the model of Eq. (3) as slightly- compressible by replacing the principal invariants I_1 and I_2 by equivalent invariant ones Simo and Hughes (1998). Consequently, the strain-energy density function has been decomposed as the sum of the two energies related to distortional and dilatational deformations, so that Eq. (3) becomes

$$\Psi = \tilde{\Psi}(\bar{I}_1, \bar{I}_2) + \hat{\Psi}(J), \tag{18}$$

where $\bar{I}_1 = I_1/I_3^{1/3}$ and $\bar{I}_2 = I_2/I_3^{2/3}$.

We point out that, $\tilde{\Psi}(\bar{I}_1, \bar{I}_2) = \frac{\mu_0}{2}\alpha(\bar{I}_1 - 3) + (1 - \alpha)(\bar{I}_2 - 3)$ and $\hat{\Psi}(J) = \frac{\kappa_0}{2}(J - 1)^2$ where κ_0 is the bulk modulus. We have implemented the strain-energy density function of Eq. (3) in a FE code.

The material parameters $c_{10} = \alpha\mu_0/2$ and $c_{01} = (1 - \alpha)\mu_0/2$ are of a Silicone rubber Seibert et al. (2014) (see, Table I); i.e. the constants of Mooney-Rivlin model Mooney (1940).

A secure bond between the sample and the clamps can be challenging to achieve experimentally. Indeed, the material response is sensitive to gripping techniques used to apply the loads. For instance, the sandpaper could be incorporated if slippage presented a problem. These techniques can also minimize the amount of clamping pre-strain that causes the bulging toward the sample center and outside of the clamps. Therefore, effects from the free and clamped edges could influence the predicted strain and stress fields in the sample. Accordingly, the "perfect" boundary conditions have been assumed for the FE simulations, and these applied through the nodes that were in contact with clamps. So, two-dimensional FE-model has been used by considering plane-stress condition; which is consisting of quadrilateral elements with two degrees of freedom at each node. Each node has two in-plane translational degrees of freedom corresponding to the vertical (axial) direction and horizontal (transversal) direction. The meshing and the boundary conditions are shown in Figs. 3, along the bottom surface of the plate (in $Y = 0$), the displacements of nodes were fixed at zero in all directions. Along the top surface of the plate (in $Y = H$), we have applied the displacements to all nodes, where $u_X = U \cos \Theta$ and $u_Y = U \sin \Theta$ are respectively, the axial and transversal component. The normalized displacement $\gamma = U/H$ was incrementally increased for each value Θ ($0 < \Theta < \pi/2$). The finite element meshes of the deformed specimen are shown in Fig. 4. The FE-simulations seem not be able to predict the shape deformed at the corners of the sample probably due to the bending. Indeed, near the bonding surfaces, the bending deformation could dominate those resulting from the stretching and shearing, especially at small strains ($\gamma << 1$ and $\Theta \to 0$ deg.). The bending seems to decrease significantly at large strains (for instance $\gamma \geq 4$ and $\Theta \to 0$ deg.), so that, the stretching and shearing strains may co-exist, and are depending on Θ. Anyway, there was a small core area in which the strains were homogeneous; with any "digital image correlation" measurement systems, it is straightforward to determine the in-plane components of the deformation gradient. We may assume that the corresponding stress distribution vary in same way for homogeneous, elastic materials. Therefore, we may establish a relationship between the local stresses in central region and applied forces on the clamp edges of the sample. We represent respectively, in Figs. 5, the graphs of normal and shear Cauchy stress distributions in core region arising from the FE- simulations and analytically computed. A good agreement was obtained for moderate strains, i.e. $\gamma \leq 2$.
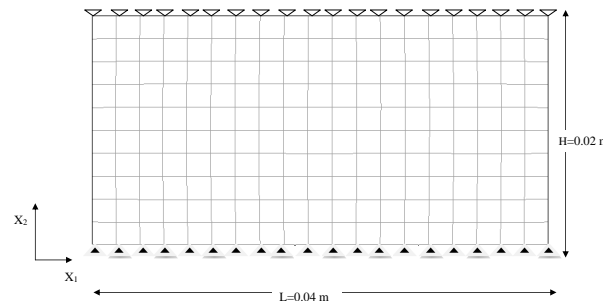
Fig. 3: Mesh and boundary conditions for FE analysis of the shearing/stretching test specimen. The boundary conditions of the test are symbolized by $\triangledown$ a displacement is imposed on the nodes along the top surface of the specimen, and $\blacktriangle$ the displacements at the nodes of the bottom surface are fixed at zero in all directions.

Tab. 1: Model parameters values

parameter	value
c_{10} [MPa]	0.111
c_{01} [MPa]	0.039
μ_0 [MPa]	0.9
κ_0 [MPa]	2000

(a) $\Theta = 5$; $\gamma = 2$ (b) $\Theta = 17$; $\gamma = 2$ (c) $\Theta = 30$; $\gamma = 2$

(d) $\Theta = 5$; $\gamma = 4$ (e) $\Theta = 17$; $\gamma = 4$ (f) $\Theta = 30$; $\gamma = 4$
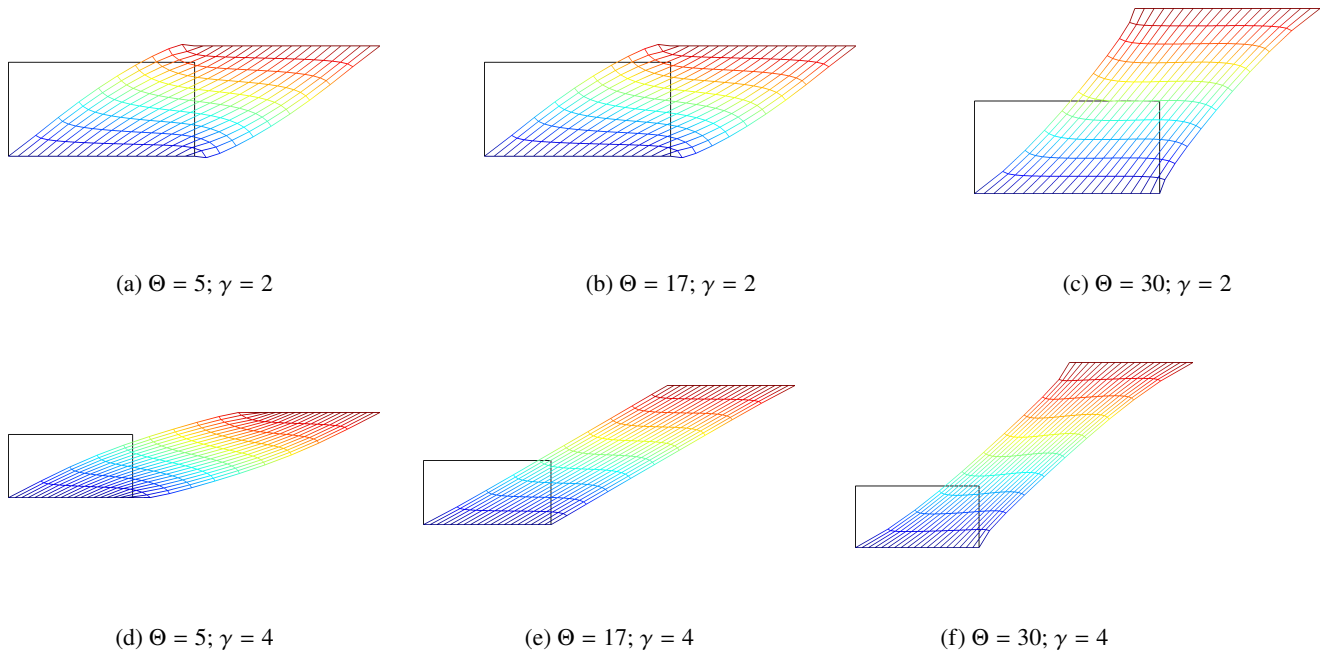
Fig. 4: Mesh and shape of the deformed sample for $\Theta = 5$, 17 and 30 $deg.$; $\gamma = 2$ and 4.

(a)   (b)
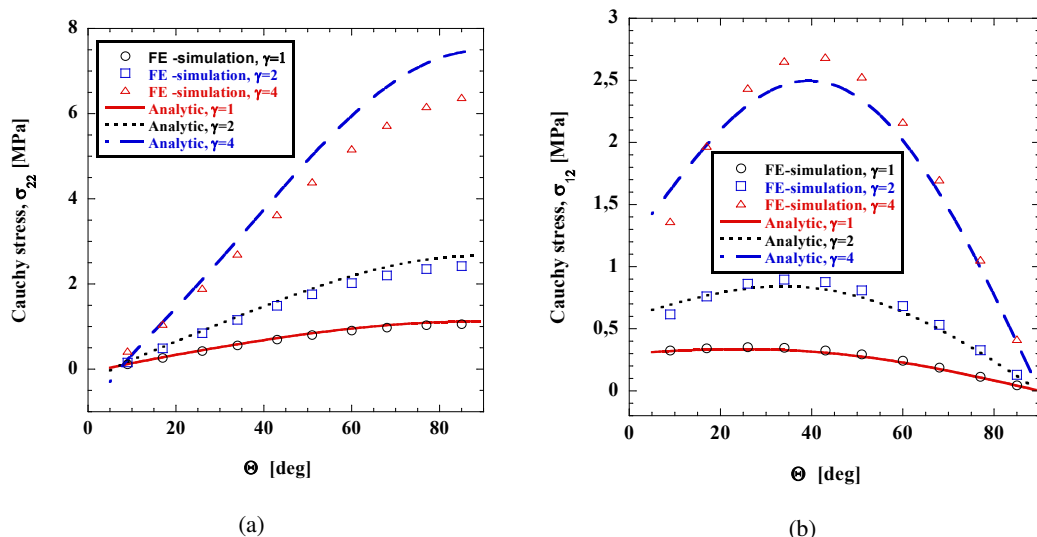
Fig. 5: Graphs of the Cauchy stresses vs. for $\gamma = 2$ and 4 in the core region of the sample, inferred from Eqs. (9), (10) and (11) and of that arising from the FE simulations.

5 Conclusion

In this work, we have presented the design of a novel testing in order to characterize the multi-axial behavior of elastomeric materials. The stress-strain responses depend on both the stretching-direction and amplitude of displacement prescribed on the edge of the sample. We show that, the strain and stress fields are quasi-homogeneous in core region of the sample. So, the experimental data arising from this test could be suitable for identification or/and validation of hyperelastic models. As consequence, this test could be representing an alternative to tensile and rectilinear shear testing performed separatley.

Acknowledgment

References

H. Baaser, Ch. Hopmann, and A. Schobel. Reformulation of strain invariants at incompressibility. *Arch. Appl. Mech.*, 83(2): 273–280, 2013.

A Bertram. *Elasticity and Plasticity of Large Deformations: An Introduction*. 2nd Edition, Springer, 2008.

M. Destrade, J.G. Murphy, and G. Saccomandi. Simple shear is not so simple. *Int. J. of Nonlinear Mech.*, 47:210–214, 2012.

C. Galliot and R.H. Lushinger. Uniaxial and biaxial mechanical properties of ETFE foils. *Polym. Testing*, 30(4):356–365, 2011.

M. Grédiac, Pierron F., S. Avril, and E. Toussaint. The virtual fields method for extracting constitutive parameters from full-field measurements. *a review, Strain*, 42(4):233–253, 2006.

Z. Guo and L.J. Sluys. Application of a new constitutive model for the description of rbber-like materials under monotonic loading. *Int. J. Solids and Struct.*, 43(9):2799–2819, 2006.

S. Hartmann and S. Rodriguez. in Advanced Strutural Materials. *Springer International Publishing, Cham*, 80, 2018.

S. Hartmann, R.R. Gilbert, and C. Sguazzo. Basic studies in biaxial tensile tests. *GAMM-Mutteilungen*, 41(1), 2018. doi: 10.1002/gamm.201800004.

F. Hild and S. Roux. Digital image correlation: from displacement measurement to identification of elastic properties. *a review, Strain*, 42(2):69–80, 2006.

G. Holzapfel. *Nonlinear Solid Mechanics*. ISBN-471-82304, Wiley, 2000.

C.O. Horgan and Murphy J.G. Simple shearing of incompressible and slightly compressible isotropic nonlinearly elastic materials. *J. Elast.*, 98:205–221, 2014.

C.O. Horgan and M. Smayda. The importance of the second strain invariant in the constitutive modeling of elastomers and soft biomaterials. *Mech. Mater.*, 51:43–52, 2012.

H. Lee. Elastic-plastic deformation at finite strains. *Jurnal of Applied Mechanics*, 36:1–14, 1969.

V.A. Lubarda. Constitutive theories based on the multiplicative decomposition of deformation gradient: Thermoelasticity, elastoplasticity and biomechanics. *Appl. Mech. Rev.*, 57(2):95–108, 2004.

L.A Mihai and A. Goriely. Finite deformation in cellular with hyperelastic cell walls. *Int. J. Solid and Struct.*, 53:107–128, 2015.

M. Mooney. A theory of Large Elastic Deformation. *J. Appl. Phys.*, 11(9):582–592, 1940.

R.W. Ogden. *Nonlinear Elastic Deformations*. Dover Publications Inc. Mineola, New York, 1997.

N Promma, B. Raka, M. Grédiac, E. Toussaint, J-B. Le Cam, X. Blanchard, and F. Hild. Application of the virtual fields method to mechanical characterization of elastomeric materials. *Int. J. Solids and Struct.*, 46:698–715, 2009.

S. Reese and S. Govindjee. A theory of finite viscoelasticity and numerical aspects. *Int. J. Solid and Struct.*, 35:3455–3482, 1998.

M. Sasso, G. Palmieri, G. Chiappini, and D. Amodio. Characterization of hyperelastic rubber-like materials by biaxial and uniaxial stretching tests based on optical methods. *Polym. Testing*, 27:995–1004, 2008.

H. Seibert, H. Schreffer, and S Diebels. Biaxial testing of elastomers-Experimental setup, measurement and experimental optimisation of specimen's shape. *Techishche Mechanik*, 34:72–89, 2014.

J.C. Simo and T.J.R. Hughes. *Computational Inelasticity*. Springer, New York, 1998. doi: 10.1007/978-1-4612-0555-5.

J. Thiel, C.and Voss, R. Martin, and P. Neff. Shear, pure and simple. *Int. J. of Nonlinear Mech.*, 112:57–72, 2019.

A. Wineman and M. Ghandi. On local and global universal relations in elasticity. *J. Elast.*, 14:97–1029, 1984.